NRIAG Journal of Astronomy and Geophysics (2016) 5, 277–288

National Research Institute of Astronomy and Geophysics

NRIAG Journal of Astronomy and Geophysics

www.elsevier.com/locate/nrjag

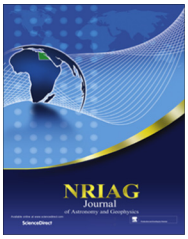

The fundamental plane of early-type galaxies in different environments

R.M. Samir [a,*], F.M. Reda [a], A.A. Shaker [a], A.M.I. Osman [a], M.Y. Amin [b,c]

[a] *National Research Institute of Astronomy and Geophysics (NRIAG), 11421 Helwan, Cairo, Egypt*
[b] *Physics Dept., College of Sci. Humanities-Hawtat Sudair, Majmaah Univ., Saudi Arabia*
[c] *Astronomy, Space Science and Meteorology Dept., Cairo University, Egypt*

Received 19 May 2015; revised 19 May 2016; accepted 23 June 2016
Available online 25 July 2016

KEYWORDS

Early-type galaxies;
The fundamental plane;
The Kormendy relation;
The Faber-Jackson relation;
Shells;
Tidal tails

Abstract The study of Early-Type Galaxies (ETGs) in different environments is a strong tool to understand their star formation history and their evolution. The Fundamental Plane (FP) of ETGs has been studied in different environments in the nearby universe such as in groups, clusters and the field. We found that our sample of ETGs in different environments shows a good agreement with the FP of Coma cluster, except for a scatter of some galaxies. A major part of the scatter in the FP is due to variations in mass to light ratio as a result of metallicity or age trends in the stellar populations and structural or dynamical properties of galaxies. We noticed that the most deviant galaxies from the FP show many fine structures as tidal tails, shells, dust and a kinematically distinct core which indicates a past merger involving at least one gas-rich progenitor.

1. Introduction

Early-Type galaxies (ETGs) represent a group which includes both elliptical (E0–E7) and lenticular (S0) galaxies. They represent a class of well studied objects both because of their homogeneous properties and their high luminosities ($-24 \leqslant M_B \leqslant -20$) which allows to detect them at large distances. They are specifically important as they contain most of the visible mass in the universe (for a detailed review, see Renzini, 2006, and references therein). Therefore, by understanding their evolution, we can understand the evolution of galaxies in general, and the evolution of the universe as a whole.

Although ETGs seem to be a nearly homogeneous class, the data collected in the last 30 years showed that there are significant departures from the general properties found in the form of large quantities of gas and dust (Capaccioli and Longo, 1994; Goudfrooij et al., 1994a,1994b), counter rotating nuclei and polar rings (Bender, 1988; Whitmore et al., 1987), shells, ripples, and disky or boxy components (e.g. Malin and Carter, 1980; Schweizer, 1980; Schweizer et al., 1990) and distinctive tidal tails (Fort et al., 1986; Schweizer and Seitzer, 1992; Michard and Prugniel, 2004; Bennert et al., 2008; Tal et al., 2009; Janowiecki et al., 2010). These morphological

* Corresponding author.
Peer review under responsibility of National Research Institute of Astronomy and Geophysics.

Production and hosting by Elsevier

http://dx.doi.org/10.1016/j.nrjag.2016.06.004

structures are explained in most of the theoretical models as a result of past merging in early stages of galaxy formation or of tidal interactions with close neighbors (e.g., de Zeeuw and Franx, 1989; Franx et al., 1989).

The role that environment plays in shaping the properties of ETGs is still an open issue in our understanding of galaxy formation and evolution (see Conselice et al., 2013 as a recent review). It is accepted that galaxy encounters, merging and interaction with inter cluster medium (ICM) are all processes that affect on the properties of galaxies to some extent. The influence of environment on the evolution of galaxies is testified by the presence of the well-known morphology-density relation (Dressler, 1980), according to which ETGs are preferred to be found in high density environments (Postman and Geller, 1984; Dressler et al., 1997; Postman et al., 2005; Bamford et al., 2009), while late-type galaxies are more found in low density environments. This distribution was proved in many studies: for example, Calvi et al. (2012) showed that there is a smooth increase in the fraction of ETGs when going from single galaxies, to pairs, to groups. Another relation that shows the influence of environment is the star formation-density relation (Lewis et al., 2002; Gómez et al., 2003; Haines et al., 2007).

The study of galaxies in different environments is a robust tool to understand their evolution and star formation history (e.g., Kuntschner et al., 2002; Sánchez-Blázquez et al., 2003, 2006; Thomas et al., 2005; Collobert et al., 2006). ETGs display a relation in the 3-dimensional parameter space among their effective radius r_e, the central velocity dispersion σ_o and the luminosity L (or equivalently the effective surface brightness expressed as I_e in linear flux units, where $I_e = L/(2\pi r_e^2)$, or μ_e in magnitudes). They are concentrated on a plane called the fundamental plane (FP, Dressler et al., 1987; Djorgovski and Davis, 1987) with,

$$r_e \propto \sigma_o^a \langle I_e \rangle^b \quad (1)$$

Which can be written as,

$$\log r_e = a \log \sigma_o + b\langle \mu_e \rangle + c \quad (2)$$

where a and b are the slopes and c is the offset (intercept) of the FP. $\langle \mu_e \rangle$ is the mean effective surface brightness enclosed by r_e (simply referred to as the mean surface brightness). The exponents a and b depend on the specific band used for measuring the luminosity. This indicates that, besides being in virial equilibrium, ETGs show striking regularity in their structures and stellar populations (Renzini and Ciotti, 1993; Borriello et al., 2003).

The FP can be understood as a demonstration of the virial plane predicted for relaxed systems (Binney and Tremaine, 2008), with assuming that galaxy mass-to-light ratios (M_{dyn}/L) are constant or smoothly varying for galaxies. If M_{dyn}/L is constant and if the structures were homologous for all ETGs, then the FP would be equivalent to the virial plane which takes the form $r_e \propto \sigma^2 \langle \mu_e \rangle^{-1}$ with coefficients of $a = 2$ and $b = -1$ (Faber et al., 1987). Otherwise, the FP is rotated from the virial plane and the tilt of the FP is the difference between the observed coefficients of the plane, a and b, and those from the virial plane. Jørgensen et al. (1996) found that $r_e \propto \sigma^{1.24} I_e^{-0.82}$ for the FP of local cluster ETGs. Also Pahre et al. (1998) found that the slopes, $a \sim 1.53$ and $b \sim -0.79$ for ellipticals observed in the near-infrared. The FP represents an important tool to study the properties of early type and dwarf galaxies and compute cosmological parameters. It is also an important diagnostic tool for galaxy evolution and mass-to-light (M/L) variations with redshift.

Although the FP relation is quite tight, there is a significant scatter around the plane and there is some contradiction in the literature regarding the source of this scatter. Some studies found that the scatter could be due to some reasons, such as variations in the formation times of galaxies, differences in the dark matter content of galaxies or metallicity trends in stellar populations. According to observations, the scatter around the FP is very low, and the position of a galaxy above or below the plane is independent of galaxy flattening, velocity anisotropy and isophotal twisting.

Faber et al. (1987) found that deviations from the FP can be formed by M/L variation due to e.g. metallicity or age trends in stellar populations, dynamical or structural properties, and relative distribution of dark matter. In fact, each of these effects may also introduce a tilt into the FP if they represent a function of elliptical galaxy mass.

The origin of the scatter around the FP has been investigated by many authors. Jørgensen et al. (1996) could not reduce the scatter around the FP by introducing additional parameters, such as isophotal shape of the galaxies or ellipticity. Other studies found that variations in stellar populations in ETGs are partially responsible for the intrinsic scatter (e.g. Gregg, 1992; Guzmán and Lucey, 1993; Guzmán et al., 1993). Forbes et al. (1998) found that the scatter of the FP for a sample of non cluster galaxies is partly due to variation in galaxy age at a given mass, and to variations in the time of the last starburst. Also Reda et al. (2005) found the same results by studying a sample of isolated galaxies. They found that some galaxies deviate from the FP having lower M/L ratio and they explained this as due to younger stellar populations of those galaxies, probably induced by recent gaseous merger. Other studies showed that a major part of the scatter in the FP is due to variations in M/L ratio (e.g., Cappellari et al., 2006; Bolton et al., 2008; Auger et al., 2010; Cappellari et al., 2013).

On the other hand, some studies (e.g., Magoulas et al., 2012) found that the age of galaxies is the most important source of offset from the FP and may drive other trends through its correlation with environment, morphology and metallicity.

The FP appears to be the same in all environments (universal), in the sense that the coefficients are similar for galaxies in environments ranging from high density clusters to the low-density field (de la Rosa et al., 2001; Reda et al., 2005; Holden et al., 2010). On the other side, there are suggestions in the literatures that there are moderate, but significant, environmental variations (e.g. Lucey et al., 1991; de Carvalho and Djorgovski, 1992; Bernardi et al., 2003; La Barbera et al., 2010a, 2010b; Ibarra-Medel and López-Cruz, 2011). On the other side, Cappellari et al. (2013) showed that the larger scatter in the FP is due to stellar population effects. They also confirmed that the deviation of the FP coefficients from the virial plane is due to M/L variation.

The aim of this study was to investigate the effect of local environment on the properties of early-type galaxies, in particular their scaling relations using a sample of ETGs in different environments such as in groups, clusters and in the field. In Section 2, we present the data used in this study that comes from photometric and spectroscopic observations of galaxies

at $0 < z < 0.08$. Section 3 presents our results concerning the fundamental plane, the Kormendy relation and the Faber-Jackson relation of ETGs. In Section 4, we discuss our results. Section 5 summarizes our main conclusions.

2. The data

In our study we used a sample consisting of 94 ETGs collected from different sources from literature as follows: 64 galaxies from Annibali et al. (2010, sample 1), 20 galaxies from Koleva et al. (2011, sample 2) and 10 galaxies from Mármol-Queraltó et al. (2009, sample 3). Their effective radii (r''_e) and central velocity dispersions (σ_o) are published by the authors. Their mean surface brightnesses $\langle\mu_e\rangle_B$ are calculated following Graham and Driver (2005). Effective radii were converted from arcsecond to parsec at the distance of the galaxy assuming that the Hubble constant $H_0 = 75\ \mathrm{km\ sec^{-1}\ Mpc^{-1}}$.

Sample 1 consists of 64 galaxies from Annibali et al. (2010), mostly located in low density environments (see Table 1). All galaxies in this sample belong to the *Revised Shapley Ames Catalog of Bright Galaxies* (RSA) (Sandage and Tammann, 1987) and have redshift lower than $\sim$5500 km s^{-1}. For this sample the effective radii in arcsec are obtained from RC3 (de Vaucouleurs et al., 1991) and the σ_o is from HyperLeda database (http://leda.univ-lyon1.fr/). The values of σ_o are obtained from apertures in $r_e/8$ region.

Sample 2 consists of 20 galaxies from Koleva et al. (2011). Their basic properties are summarized in Table 2. Eight of these galaxies are in The Fornax cluster and 12 galaxies are in the Virgo cluster. For this sample the values of σ_o are from HyperLeda. For galaxies in the Fornax cluster, the velocity dispersion is overestimated in the external regions and more importantly, it is underestimated in the central regions.

Sample 3 consists of 10 galaxies (see Table 3). Two of them are in the Fornax cluster and 8 galaxies are in the field or low density environment. This sample is selected from Mármol-Queraltó et al. (2009). Their r_e values in arcsec in the B-band and their σ_o are obtained through private communication with Mármol-Queraltó, where they collect them from the literature.

3. Results

Table 4 lists the calculated logarithmic values for the photometric and spectroscopic parameters of our samples in addition to the mean surface brightness $\langle\mu_e\rangle_B$.

3.1. The fundamental plane in log (r_e), $\langle\mu_e\rangle$, and log (σ_o) space

Fig. 1 shows the FP of our samples of ETGs in different environments. The edge-on projection of the FP of Coma cluster is represented by a solid line, while the dashed line represents the 1σ dispersion of galaxies in Coma cluster. Our samples of ETGs are illustrated using different symbols for different references as shown in Table 4. It is clear in this Figure that most of the deviant galaxies from the FP are those of sample 2 in Virgo and Fornax clusters which are located below it. As mentioned in Section 3, the values of σ_o for the Fornax galaxies are underestimated and this can be responsible for their direction of scatter relative to the FP. For the other galaxies, many different reasons can cause them to show such significant deviation. For example, the projection effects can be reflected on a large spread in the measurement of σ_o. Also, σ anomalies and the presence of inner subcomponents such as disks or central black holes (e.g., D'Onofrio et al., 1997; Goudfrooij et al., 2004) and the effects of aperture sizes must be taken into account.

In the next subsections we will analyze the available scaling relations such as the fundamental plane in κ-space, the Kormendy relation and the Faber-Jackson relation to introduce some reasonable explanation for the observed scatter of our sample galaxies about the FP.

In Fig. 2, we performed fitting for our sample using the least square method and we obtained the parameters a, b and c of the FP as follows: $a = 1.235$ with error 0.608, $b = 0.222$ with error 0.107 and $c = -3.983$ with error 2.145. It is clear that the values of a and b of our fitting are close to those of the Coma cluster, while the value of parameter c is somehow different.

3.2. The fundamental plane in κ-space

By a simple orthogonal coordinate transformation (i.e., a rotation), a different expression for the FP in terms of kappa (κ) space was introduced by Bender et al. (1992). The axes of this coordinate system are directly proportional to the physical parameters of galaxies and defined as

$$\kappa_1 = \frac{2\log(\sigma) + \log(r_e)}{\sqrt{2}} \tag{3}$$

$$\kappa_2 = \frac{2\log(\sigma) + 2\log(I_e) - \log(r_e)}{\sqrt{6}} \tag{4}$$

$$\kappa_3 = \frac{2\log(\sigma) - \log(I_e) - \log(r_e)}{\sqrt{3}} \tag{5}$$

where $\log I_e = -0.4(\langle\mu_e\rangle - 27)$, κ_1 is proportional to the logarithm of the mass, κ_2 is proportional to the logarithm of $(M/L)\,I_e^2$ and κ_3 is proportional to the logarithm of M/L. The edge-on view of the FP is represented by κ_1 and κ_3.

In Fig. 3 we show the distribution of our sample of ETGs in κ_1–κ_3 space. They show a similar tilt and dispersion to those of Virgo cluster galaxies from Bender et al. (1992). The galaxies that show deviation above the FP in Fig. 1 also show a tendency to have larger values of κ_3 i.e. larger M/L ratios as expected for their old ages. On the other side, the galaxies that are deviated below the FP in Fig. 1 also show a tendency to have smaller values of κ_3 which indicate lower M/L ratios. Previous studies (e.g. Forbes et al., 1998) show that there is a correlation between the residuals from the FP and the age of the central stellar populations of the galaxies. Table 5 shows the available published ages for some of our sample galaxies. These published ages are luminosity-weighted central ages based on Lick absorption lines and single stellar population models to break the age-metallicity degeneracy.

3.3. The Kormendy relation

Fig. 4 shows the Kormendy relation (KR) between the mean surface brightness within the effective radius $\langle\mu_e\rangle_B$ and effective radius in the B-band of our galaxies. The solid line represents the Hamabe and Kormendy (1987) relation,

Table 1 Main characteristics of Sample 1 (Annibali et al., 2010). Col. (1) gives the galaxy identification; Col. (2) provides the galaxy morphological classification according to RC3 (Third Reference Catalog of bright galaxies, de Vaucouleurs et al., 1991); Col. (3) gives the effective radius r_e in seconds of arc from RC3; Col. (4) gives the central velocity dispersion σ_o in km s^{-1} from HyperLeda (http://leda.univ-lyon1.fr//); Col. (5) indicates the environment of the galaxy collected by us (when available, the name of the environment is mentioned): when the galaxy is a member of a well known cluster or group, their names are indicated; when the galaxies do not belong to a cluster or a group, it is labeled as field galaxy. The term "low density" refers to the richness parameter of galaxies as clarified by Annibali et al. (2010).

Galaxy	Type RC3	r_e (arcsec)	σ_o (km s^{-1})	Environment
NGC 128	S0	17.3	183.0	
NGC 777	E1	34.4	317.0	Group (LGG 42)[a]
NGC 1052	E4	33.7	215.0	Group (LGG 71)[a]
NGC 1209	E6	18.5	240.0	Group[b]
NGC 1297	SAB0	28.4	115.0	Low density
NGC 1366	S0	10.6	120.0	Fornax and Eridanus Cloud[c]
NGC 1380	SA0	20.3	240.0	Fornax Cluster
NGC 1389	SAB(s)0	15.0	139.0	Fornax and Eridanus Cloud[c]
NGC 1407	E0	70.3	286.0	Eridanus group (LGG 100)[a]
NGC 1426	E4	25.0	162.0	Low density
NGC 1453	E2	25.0	162.0	Group (LGG 103)[a]
NGC 1521	E3	25.5	235.0	
NGC 1533	SB0	30.0	174.0	Dorado Cloud[c]
NGC 1553	SA(r)0	65.6	180.0	Dorado Cloud[c]
NGC 1947	S0	32.1	142.0	Low density
NGC 2749	E3	33.7	248.0	
NGC 2911	SA(s)0	50.9	235.0	Group (LGG 177)[a]
NGC 2962	RSAB(rs)0+	23.3	180.0	
NGC 2974	E4	24.4	220.0	Group (LGG 179)[a]
NGC 3136	E:	36.9	230.0	Low density
NGC 3258	E1	30.0	271.0	Antlia Hydra Cloud[c]
NGC 3268	E2	36.1	227.0	Antlia Hydra Cloud[c]
NGC 3489	SAB(rs)	20.3	129.0	Low density
NGC 3557	E3	30.0	265.0	Antlia Hydra Cloud[c]
NGC 3607	SA(s)0:	43.4	220.0	Field[a]
NGC 3818	E5	22.2	191.0	Field[b]
NGC 3962	E1	35.2	225.0	Crater cloud[c]
NGC 4374	E1	50.9	282.0	Virgo, group (LGG 292)[a]
NGC 4552	E	29.3	264.0	Virgo cluster[c]
NGC 4636	E0−1	88.5	209.0	Virgo cluster[c]
NGC 4696	E+1	85.0	254.0	Centaurus Cloud[c]
NGC 4697	E6	72.0	174.0	Cluster (Virgo)[a]
NGC 5011	E1−2	23.8	249.0	Centaurus Cloud[c]
NGC 5044	E0	82.3	239.0	Virgo cluster[c]
NGC 5077	E3+	22.8	260.0	Virgo cluster[c]
NGC 5090	E2	62.4	269.0	Centaurus Cloud[c]
NGC 5193	E pec	26.7	209.0	
NGC 5266	SA0-	76.7	199.0	Low density
NGC 5328	E1:	22.2	303.0	NGC 5328 group
NGC 5363	S0-a	36.1	199.0	Group (LGG 362)[a]
NGC 5638	E1	28.0	168.0	Group (LGG 386)[a]
NGC 5812	E0	25.5	200.0	Field[a]
NGC 5813	E1−2	57.2	239.0	Group (LGG 393)[a]
NGC 5831	E3	25.5	164.0	Group (LGG 393)[a]
NGC 5846	E0+	62.7	250.0	Group (LGG 393)[a]
NGC 5898	E0	22.2	220.0	Virgo – Libra Cloud[c]
NGC 6721	E+:	21.7	262.0	
NGC 6758	E+:	20.3	242.0	
NGC 6776	E+pec	17.7	242.0	Field
NGC 6868	E2	33.7	277.0	Group[b]
NGC 6876	E3	43.0	230.0	
NGC 6958	E+	19.8	223.0	Field[b]
NGC 7007	SA0-:	15.4	125.0	Low density
NGC 7079	SB(s)0	19.8	155.0	Low density
NGC 7097	E5	18.1	224.0	Low density
NGC 7135	SA0- pec	31.4	231.0	Low density

Table 1 (*continued*)

Galaxy	Type RC3	r_e (arcsec)	σ_o (km s^{-1})	Environment
NGC 7192	E+:	28.6	257.0	Pavo – Indus Spur[c]
NGC 7332	S0 pec sp	14.7	136.0	Field[a]
NGC 7377	SA(s)0+	36.9	145.0	
IC 1459	E	34.4	311.0	Telescopium – Grus Cloud[c]
IC 2006	E	28.6	122.0	Cluster[b]
IC 3370	E2+	38.6	202.0	Centaurus Cloud[c]
IC 4296	E	41.4	340.0	
IC 5063	SA(s)0+	26.7	160.0	

[a] Denicoló et al. (2005a).
[b] Georgakakis et al. (2001).
[c] Rampazzo et al. (2013) where they took the group/cluster identification from Tully (1988).

$$\mu_e(V) = 2.94\log(r_e) + 19.48 \quad (6)$$

shifted from V to the B-band assuming typical colors of B−V = 0.9. We also transformed the surface brightness (μ_e) at r_e to $\langle\mu_e\rangle$ using the relation of Graham and Colless (1997).

As clear in Fig. 4, most of the galaxies that are scattered from the FP also show deviation from the KR.

3.4. The Faber-Jackson relation

Fig. 5 shows the correlation between the central velocity dispersion ($\log\sigma_o$) and the absolute magnitude M_B in the B-band (FJR). Our sample galaxies are represented by different symbols according to their references as previously shown in Fig. 1. As clear in Fig. 5, most of our sample galaxies follow the FJR of ellipticals as the comparison sample in spite of some galaxies which are assigned in Fig. 1 to have significant scatter. We find that most of the galaxies which are scattered in Fig. 1 also show significant dispersion in this relation too.

Forbes and Ponman (1999) studied 5 galaxies of our sample. Those galaxies are NGC 4261, NGC 4697, FCC 021 (NGC 1316), FCC 170 (NGC 1381) and FCC 177 (NGC 1380A). They found that a galaxy's position relative to the FJR depends on its age. In particular, younger ellipticals are systematically brighter in M_B and/or have lower central velocity dispersion (σ_o).

4. Discussions

In Figs. 1 and 2 we have compared the FP for our sample of ETGs in different environments with that for the Coma cluster ETGs and isolated galaxies. We found that the FP of Coma cluster can fit well to some reasonable extent the galaxy samples taken from Annibali et al. (2010) and Mármol-Queraltó et al. (2009) as well as the comparison sample of isolated ETGs from Reda (2007). We noticed that the most deviant galaxies from the FP are from Koleva et al. (2011). For these galaxies, there are two possible reasons for their deviation from the FP. It is clear that they are also located below the $\langle\mu_e\rangle_B$ - r_e relation (see Fig. 4). Their positions in this KR indicate less $\langle\mu_e\rangle$ than expected for their sizes. Possible reasons for such dimming measurements of $\langle\mu_e\rangle_B$ can be due to the presence of dust lanes or gas within the central regions of those galaxies. That is because of sensitivity of B-band to structures of galaxies. To explain the second reason for their deviation from the FP, we test the projection of the FP in κ-space (see Fig. 3). These galaxies also tend to have smaller κ_3 as clear in Fig. 3, which means that they have lower M/L ratios as expected for their young stellar populations (see Table 5).

In Fig. 1 some galaxies deviate above the FP, which are NGC 2911, NGC 4261, NGC 4697, NGC 1533 and VCC 0828. In Fig. 3, the same five galaxies show a tendency to have larger κ_3 values in the direction of higher M/L ratios which can be explained by the old ages of their stellar population. For example, NGC 1533 and NGC 4697 are old galaxies with ages 11.9 ± 6.9 and 10.10 ± 1.4 Gyr, respectively, while NGC 2911 has a moderate age of 5.7 ± 2 Gyr (see Table 5).

NGC 4697 has a dust lane and has a central supermassive black hole (SMBH) of mass 1.2×10^8 $M_\odot$ (Pinkney et al., 2000; Yuan et al., 2009). On the other side, many studies showed that this galaxy is candidate for a recent merger based on the presence of a central dusty disk (Pinkney et al., 2003; Sambhus et al., 2006; Bregman et al., 2006a, 2006b, 2008). From Fig. 1, it is noticed that NGC 4697 is highly deviated above the FP. This deviation could be attributed to the structures it has such as the central dust disk, the SMBH and its recent merger event. Also, its low mean effective surface brightness (21.40 mag/arcsec^2) may participate in its deviation from the FP while it is also deviated from the KR as shown in Fig. 4. Although KR indicates that larger galaxies have lower surface brightness, this galaxy is found to have much lower $\langle\mu_e\rangle$ than expected for its size. On the other hand its central velocity dispersion is consistent with its total absolute magnitude (FJR, Fig. 5). We can conclude that its $\langle\mu_e\rangle$ is likely to be the main reason of its deviation from the FP in Fig. 1. Such lower surface brightness affects the value of κ_3 toward having high M/L ratio.

NGC 4261 is an old galaxy with age of $10.6^{+4.7}_{-4.7}$, as measured by TF02 (see Table 5). This galaxy is a well known radio source in the Virgo cluster. It contains a well-defined disk of dust and gas which surrounds the unresolved nucleus. The structure and dynamics of this disk have been studied by Jaffe et al. (1993, 1996) and Ferrarese et al. (1996). In addition to this, the later authors detected a black hole with mass $\sim 5 \times 10^8$ $M_\odot$. However, dust lanes were detected roughly along the major axis (Mahabal et al., 1996). Although KR indicates that larger galaxies have lower surface brightness, this galaxy is found to have much lower $\langle\mu_e\rangle$ than expected for its size. On the other hand its central velocity dispersion is consistent with its total absolute magnitude (FJR, Fig. 5).

Table 2 Structural properties of Sample 2 (Koleva et al., 2011). Col. (1) gives the galaxy name; Col. (2) states another name for the galaxy; Col. (3) gives type of the galaxy; Col (4) states the effective radius r_e in seconds of arc; Col. (5) gives the central velocity dispersion σ_o in km s^{-1} from HyperLeda (http://leda.univ-lyon1.fr//); Col. (6) indicates the environment of the galaxy: when the galaxy is a member of a well known cluster, the cluster name is indicated; when the galaxy does not belong to a cluster or a group, it is labeled as field galaxy.

Galaxy	Other name	Type	r_e arcsec	σ_o (km s^{-1})	Environment
VCC 0575	NGC 4318	E	7.8	95	Virgo
VCC 0731	NGC 4365	E	35.1	256	Virgo
VCC 0828	NGC 4387	E	26.0	115	Virgo
VCC 1025	NGC 4434	E	10.6	120	Virgo
VCC 1146	NGC 4458	E	14.8	103	Virgo
VCC 1178	NGC 4464	E	6.0	129	Virgo
VCC 1231	NGC 4473	E	12.5	179	Virgo
VCC 1279	NGC 4478	E	17.0	144	Virgo
VCC 1297	NGC 4486B	cE	2.7	170	Virgo
VCC 1475	NGC 4515	E-S0	10.5	86	Virgo
VCC 1630	NGC 4551	E	15.0	107	Virgo
VCC 1903	NGC 4621	E	27.7	225	Virgo
FCC 021	NGC 1316	S0	46.3	226	Fornax
FCC 055	ESO358-006	S0	5.3	47	Fornax
FCC 148	NGC 1375	S0	9.1	69	Fornax
FCC 153	IC0335	S0	5.8	79	Fornax
FCC 170	NGC 1381	S0	4.3	150	Fornax
FCC 177	NGC 1380A	S0	8.7	67	Fornax
FCC 277	NGC 1428	E-S0	13.7	82	Fornax
FCC 301	ESO358-059	E-S0	3.4	49	Fornax

Table 3 Structural properties of Sample 3 (Mármol-Queraltó et al., 2009). Col. (1) gives the galaxy name; Col. (2) lists another name for the galaxy; Col. (3) presents morphological type of the galaxy; Col (4) gives the effective radius r_e in seconds of arc; Col. (5) states the central velocity dispersion σ_o in km s^{-1}; Col. (6) indicates the environment of the galaxy: when the galaxy is a member of a well known cluster, the cluster name is indicated; when the galaxy does not belong to a cluster or a group, it is labeled as field galaxy.

Galaxy	Other name	Type	r_e arcsec	σ_o (km s^{-1})	Environment
NGC 1379		E	23.30[1]	116.8 ± 3.6[a]	Fornax cluster[c]
NGC 1404		E	23.00[1]	244.9 ± 8.2[a]	Fornax cluster[c]
NGC 3605		E4-5	17.26[2]	91.0 ± 1.5[b]	LGG 237 group[b]
NGC 4261		E2-3	38.65[2]	302.7 ± 1.7[b]	LGG 278 group[b]
NGC 4564		E6	21.63[2]	171.1 ± 0.8[b]	LGG 289 group[b]
NGC 4742		E4	11.67[2]	91.9 ± 0.5[b]	LGG 307 group[b]
NGC 5796		E	18.50[2]	273.6 ± 2.5[b]	LGG 386 group[b]
ESO382-G16	LDR 22[c]	E	13.20[3]	237.2 ± 5.7[c]	Field[c]
ESO446-G49	LDR 34[c]	S0	19.10[3]	143.7 ± 2.0[c]	Field[c]
ESO503-G12	LDR 09[c]	E	10.64[4]	146.8 ± 2.6[c]	Field[c]

[1] Caon et al. (1994).
[2] Burstein et al. (1987).
[3] Lauberts and Valentijn (1989).
[4] RC3 (Third Reference Catalog of bright galaxies, de Vaucouleurs et al., 1991).
[a] Kuntschner (2000).
[b] Sánchez-Blázquez et al. (2006).
[c] Kuntschner et al. (2002).

From that we conclude that its $\langle\mu_e\rangle$ might be the main reason of its deviation from the FP in Fig. 1. Such lower surface brightness affects the value of κ_3 toward having high M/L ratio.

On the other hand, some galaxies are deviated below the FP as clear in Fig. 1. These galaxies are FCC 021, FCC 055, FCC 153, FCC 170, FCC 177, FCC 301, VCC 1231, NGC 1366 and NGC 4742. They also tend to have smaller κ_3 as clear in Fig. 3, which means that they have lower M/L ratios as expected for their young stellar populations (see Table 5).

FCC 021 (NGC 1316) is deviated below the FP in Fig. 1. In Fig. 3, it shows smaller κ_3 in the direction of smaller M/L ratio as expected for its young age of 3.4 Gyr as recorded by TF02 (see Table 5). This galaxy exhibits many unusual features for elliptical galaxies, such as dust patches, ripples and loops, Hα filaments (Schweizer 1980, 1981; Carter et al., 1983) and it contains a complex net of dark, dust features. The presence

Table 4 Structural properties of ETGs. The columns are as follows: identification of the galaxies, redshift for the galaxies from NED (Nasa Extragalactic Database), apparent magnitude in B-band from HyperLeda database, absolute magnitude in B-band from HyperLeda database, log of the effective radius in parsec, log of the central velocity dispersion in km/s, mean effective surface brightness in B-band, sample source: 1 – Annibali et al. (2010), 2 – Koleva et al. (2011), 3 – Mármol-Queraltó et al. (2009).

Galaxy	z	m_B (mag)	M_B (mag)	log r_e (pc)	log σ_o (km/s)	$\langle\mu_e\rangle_B$ (mag/arcsec^2)	Sample source
NGC 128	0.014146	12.46	−21.47	3.67	2.26	20.64	1
NGC 777	0.016728	12.22	−22.13	4.05	2.50	21.90	1
NGC 1052	0.005037	11.32	−20.20	3.47	2.33	20.95	1
NGC 1209	0.008673	12.15	−20.65	3.47	2.38	20.48	1
NGC 1297	0.005290	12.98	−18.63	3.41	2.06	22.24	1
NGC 1366	0.004106	12.73	−18.33	2.87	2.08	19.85	1
NGC 1379	0.004416	11.77	−19.21	3.22	2.06	20.60	3
NGC 1380	0.006261	10.80	−21.12	3.33	2.38	19.33	1
NGC 1389	0.003072	12.36	−17.70	2.84	2.14	20.23	1
NGC 1404	0.006494	10.81	−20.20	3.41	2.39	19.61	3
NGC 1407	0.005934	10.38	−21.49	3.87	2.45	21.61	1
NGC 1426	0.004813	12.20	−19.21	3.31	2.21	21.18	1
NGC 1453	0.012962	12.07	−21.64	3.79	2.21	21.05	1
NGC 1521	0.014153	12.19	−21.67	3.82	2.37	21.22	1
NGC 1533	0.002635	11.71	−17.81	2.99	2.24	21.09	1
NGC 1553	0.003602	10.20	−20.40	3.57	2.25	21.28	1
NGC 1947	0.003669	11.41	−19.19	3.26	2.15	20.94	1
NGC 2749	0.013976	12.56	−21.39	3.96	2.39	22.19	1
NGC 2911	0.010617	12.53	−20.82	4.03	2.37	23.06	1
NGC 2962	0.006558	12.63	−19.67	3.47	2.25	21.46	1
NGC 2974	0.006401	11.61	−20.55	3.46	2.34	20.54	1
NGC 3136	0.005714	10.63	−21.00	3.53	2.36	20.46	1
NGC 3258	0.009313	12.11	−20.80	3.71	2.43	21.49	1
NGC 3268	0.009340	11.84	−21.07	3.79	2.35	21.62	1
NGC 3489	0.002258	12.42	−19.32	3.52	2.11	20.95	1
NGC 3557	0.010300	10.92	−22.20	3.75	2.42	20.30	1
NGC 3605	0.002365	13.06	−17.23	2.93	1.96	21.24	3
NGC 3607	0.003202	10.83	−20.04	3.45	2.34	21.01	1
NGC 3818	0.005674	12.53	−19.44	3.38	2.28	21.26	1
NGC 3962	0.006064	11.39	−20.73	3.61	2.35	21.12	1
NGC 4261	0.007465	11.24	−21.32	3.28	2.48	21.17	3
NGC 4374	0.003536	9.89	−21.14	3.55	2.45	20.42	1
NGC 4552	0.001134	10.49	−20.51	2.89	2.42	19.82	1
NGC 4564	0.003809	11.81	−19.43	3.23	2.23	20.48	3
NGC 4636	0.003129	10.29	−20.49	3.74	2.32	22.02	1
NGC 4696	0.009867	11.13	−21.94	4.19	2.40	22.77	1
NGC 4697	0.004140	10.12	−20.35	2.97	2.24	21.40	1
NGC 4742	0.004236	11.92	−22.40	2.97	1.96	19.25	3
NGC 5011	0.010537	11.91	−21.28	3.66	2.39	20.79	1
NGC 5044	0.009280	11.24	−21.69	4.15	2.38	22.81	1
NGC 5077	0.009360	12.07	−20.99	3.62	2.41	20.85	1
NGC 5090	0.011411	11.90	−21.13	4.05	2.43	22.87	1
NGC 5193	0.012379	12.28	−21.34	3.79	2.32	21.41	1
NGC 5266	0.010014	11.62	−21.44	4.15	2.30	23.04	1
NGC 5328	0.015811	12.37	−21.76	3.82	2.48	21.10	1
NGC 5363	0.003799	10.86	−20.40	3.45	2.30	20.64	1
NGC 5638	0.005591	11.99	−20.03	3.49	2.22	21.22	1
NGC 5796	0.009549	12.23	−20.80	3.54	2.44	20.56	3
NGC 5812	0.006571	11.79	−20.51	3.51	2.30	20.82	1
NGC 5813	0.006578	11.24	−21.14	3.87	2.38	22.02	1
NGC 5831	0.005524	12.15	−19.86	3.46	2.21	21.18	1
NGC 5846	0.005717	10.82	−21.34	3.87	2.40	21.80	1
NGC 5898	0.007078	11.78	−20.65	3.47	2.34	20.51	1
NGC 6721	0.014747	12.75	−21.22	3.77	2.42	21.43	1
NGC 6758	0.011355	12.27	−21.14	3.63	2.38	20.80	1
NGC 6776	0.018279	12.73	−21.70	3.78	2.38	20.96	1
NGC 6868	0.009520	11.39	−21.65	3.78	2.44	21.02	1
NGC 6876	0.013376	11.69	−21.92	4.00	2.36	21.85	1
NGC 6958	0.009050	12.07	−20.83	3.52	2.35	20.55	1

(*continued on next page*)

Table 4 (*continued*)

Galaxy	z	m_B (mag)	M_B (mag)	log r_e (pc)	log σ_o (km/s)	$\langle\mu_e\rangle_B$ (mag/arcsec^2)	Sample source
NGC 7007	0.010334	12.74	−20.40	3.46	2.09	20.67	1
NGC 7079	0.008953	12.31	−20.50	3.51	2.19	20.79	1
NGC 7097	0.008726	12.50	−20.28	3.45	2.35	20.78	1
NGC 7135	0.008819	12.63	−20.24	3.72	2.36	22.11	1
NGC 7192	0.009934	12.04	−20.96	3.70	2.41	21.32	1
NGC 7332	0.003909	11.79	−19.66	3.09	2.13	19.62	1
NGC 7377	0.011138	11.92	−21.48	3.89	2.16	21.75	1
IC 1459	0.006011	10.86	−21.15	3.56	2.49	20.54	1
IC 2006	0.004610	12.19	−18.94	3.32	2.08	21.47	1
IC 3370	0.009773	11.55	−21.48	3.84	2.30	21.48	1
IC 4296	0.012465	11.24	−22.40	3.99	2.53	21.32	1
IC 5063	0.011348	12.65	−20.69	3.74	2.20	21.78	1
VCC 0575	0.004106	14.06	−17.60	2.82	1.98	20.51	2
VCC 0731	0.004146	10.39	−20.40	3.46	2.41	20.11	2
VCC 0828	0.001574	12.82	−18.30	3.07	2.06	21.89	2
VCC 1025	0.003572	12.89	−18.80	2.89	2.08	20.01	2
VCC 1146	0.002118	12.77	−18.20	2.87	2.01	20.61	2
VCC 1178	0.004146	13.45	−17.40	2.71	2.11	19.33	2
VCC 1231	0.007485	10.91	−19.90	3.27	2.25	18.39	2
VCC 1279	0.004500	12.04	−19.00	3.21	2.16	20.19	2
VCC 1297	0.005187	14.19	−16.80	2.46	2.23	18.34	2
VCC 1475	0.003172	13.13	−17.80	2.85	1.93	20.23	2
VCC 1630	0.003909	12.87	−18.30	3.10	2.03	20.74	2
VCC 1903	0.001368	10.52	−20.30	2.97	2.35	19.73	2
FCC 021	0.005871	9.29	−22.30	3.67	2.35	19.61	2
FCC 055	0.004266	13.90	−17.50	2.55	1.67	19.51	2
FCC 148	0.002468	13.05	−18.20	2.50	1.83	19.84	2
FCC 153	0.005400	12.84	−18.50	2.72	1.90	18.65	2
FCC 170	0.005751	12.02	−19.00	2.62	2.17	17.18	2
FCC 177	0.005207	13.21	−18.10	2.87	1.82	19.9	2
FCC 277	0.005470	13.62	−17.70	3.09	1.91	21.3	2
FCC 301	0.003406	13.96	−17.40	2.25	1.69	18.61	2
ESO382-G16	0.010998	13.48	−19.82	3.43	2.37	21.08	3
ESO446-G49	0.012795	13.65	−20.10	3.67	2.16	22.05	3
ESO503-G12	0.007228	13.40	−17.60	3.14	2.16	20.53	3

of these features strongly suggests that NGC 1316 is a merger remnant (Schweizer, 1980; Bosma et al., 1985) with a tidal-tail system. Also, On the other hand, D'Onofrio et al. (1995) noticed that the central velocity dispersion in NGC 1316 is lower than that expected for a galaxy of this luminosity from the FJR (260 versus 400 km/s). This action could be due to the presence of a dynamically cold disk-like component. Another evidence is presented by Nowak et al. (2008, their Figure 8), who found indications of a younger stellar component in the center of NGC 1316. All those characteristics mentioned above such as dust, shells, loops, ripples, and tails as previously found by D'Onofrio et al. (1997) together with a velocity dispersion which is lower than that of other elliptical galaxies of similar luminosity, cause NGC 1316 to lie far off the FP.

FCC 170 (NGC 1381) is deviated below the FP in Fig. 1, while it shows smaller κ_3, in the direction of smaller M/L ratio as shown in Fig. 3. It has a luminosity weighted age of 6.6 Gyr as determined by TF02 (see Table 5). D'Onofrio et al. (1995) found that this galaxy has a small KDC inside $r \sim 6''$. On the other hand, Silva et al. (2008) found that this S0 galaxy contains X-bulge isophotal pattern, which is related to a recent dynamical encounter or merger event. This galaxy is one of the most deviated galaxies below the FP as shown in Fig. 1. This behavior may be caused by its small values of the r_e (4.3″) and the σ_o (15 km/s). Also the structures it has such as the KDC, the bar and outer rings may contribute to this deviation.

It is found that some of the deviated galaxies were previously studied by Forbes et al. (1998). These galaxies are NGC 4261, NGC 4697, FCC 021 (NGC 1316), FCC 170 (NGC 1381) and FCC 177 (NGC 1380A). They showed that the scatter about the FP of those galaxies and others is correlated with age such that young galaxies have negative residuals from the FP, while old galaxies have positive residuals.

On the other hand, Cappellari et al. (2013) constructed detailed dynamical Jeans Anisotropic models (JAM), based on the Jeans equations, for the volume limited and mass-selected ATLAS^{3D} sample of ETGs. We found that 27 of our galaxies are in their sample. They showed that the larger scatter in the FP is due to stellar population effects, variations in the M/L ratio (including trends in the stellar initial mass function [IMF]).

5. Conclusions

In this study we investigate the influence of environment on ETGs in groups, clusters and the field. We focus our study

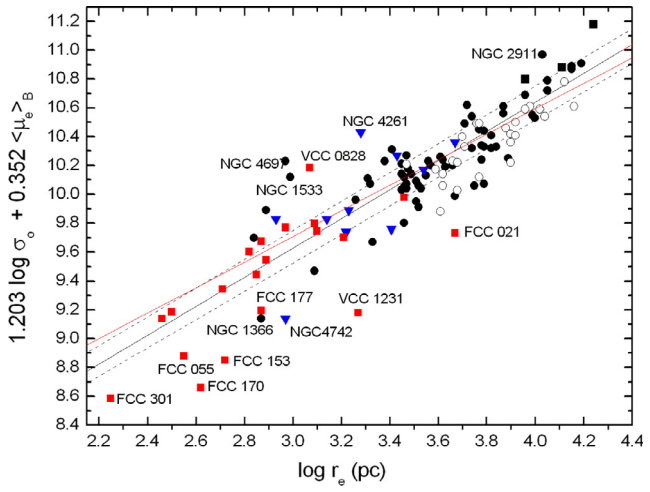

Figure 1 The FP of ETGs in different environments. The black solid line is the FP of galaxies in the Coma cluster from Jørgensen et al. (1993). The short-dashed lines represent the 1σ dispersion of galaxies in Coma cluster. The red solid line is the best linear fit for our samples. Symbols are as follows: circles: Annibali et al. (2010, sample 1), squares: Koleva et al. (2011, sample 2), down triangles: Mármol-Queraltó et al. (2009, sample 3). Open circles are for the comparison sample of isolated early-type galaxies (Reda, 2007).

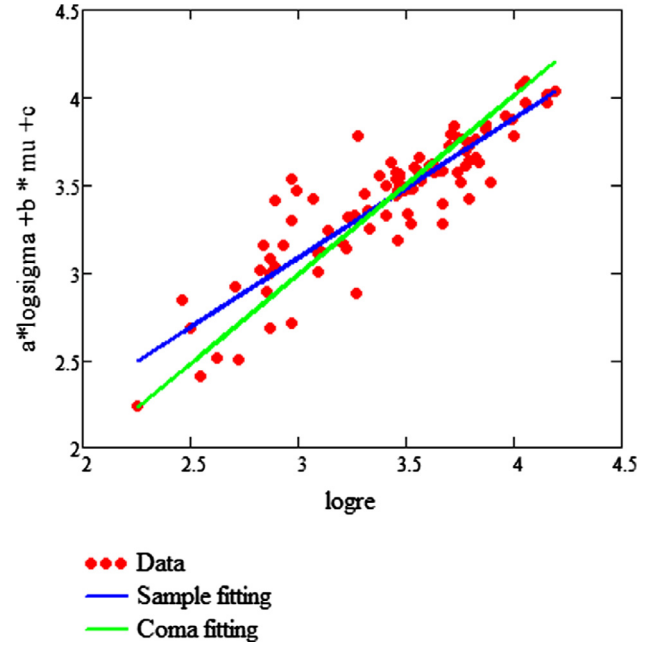

Figure 2 Fitting of the FP of ETGs in different environments. The green solid line is the FP of galaxies in the Coma cluster from Jørgensen et al. (1993). The blue solid line represents best fitting of the sample using the least square method.

on the scaling relations of ETGs such as the FP, KR and FJR. We summarize our results as follows.

As for the FP, the deviation of some galaxies above the FP is due to their large values of M/L ratios as expected for their old ages. The deviation of some other galaxies below the FP is due to having lower M/L ratios as expected for their young ages.

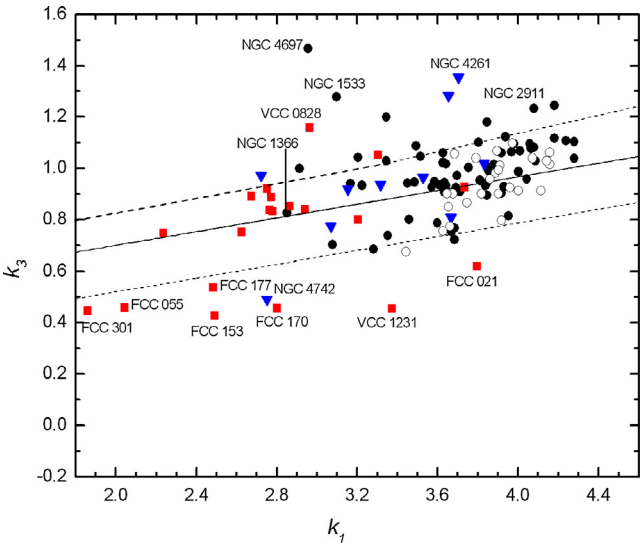

Figure 3 The edge-on view of the FP of the ETGs in different environments in the κ_1–κ_3 space. Symbols are as shown in Fig. 1. The solid line is the FP for Virgo cluster galaxies from Bender et al. (1992). The short-dashed lines represent the typical observational errors added to the 1σ intrinsic scatter of 0.05 in κ_3 for Virgo cluster galaxies (Nipoti et al., 2003). The deviant galaxies above or below the FP in Fig. 1 show a tendency to have larger or smaller values of κ_3 than the average.

Table 5 Published ages of some deviant galaxies from the FP.

Galaxy	Age (Gyr)	Reference
NGC 1366	5.9 ± 1	4
NGC 1533	11.9 ± 6.9	4
NGC 2911	5.7 ± 2	4
NGC 4261	$10.6^{+4.7}_{-4.7}$	1
NGC 4472	8.5	2
NGC 4697	10.10 ± 1.4	4
VCC 0828 (NGC 4387)	13	2
FCC 021 (NGC 1316)	3.4	2
FCC 153	3.8	3
FCC 170 (NGC 1381)	6.6	2
FCC 301 (ESO 358-G059)	5.0	3

1: Denicoló et al. (2005b, D05b).
2: Terlevich and Forbes (2002; TF02).
3: Spolaor et al. (2010).
4: Annibali et al. (2010).

We noticed that the most deviant galaxies from the FP are from Koleva et al. (2011). For these galaxies, there are two possible reasons for their deviation from the FP. It is clear that they are also located below the $\langle\mu_e\rangle_B$ - r_e relation toward less $\langle\mu_e\rangle$ than expected for their sizes. Possible reasons for such dimming measurements of $\langle\mu_e\rangle_B$ can be due to the presence of dust lanes or gas within the central regions of those galaxies. That is because of the sensitivity of B-band to structures of galaxies. The second reason for their deviation from the FP comes from their tendency to have smaller κ_3, which means

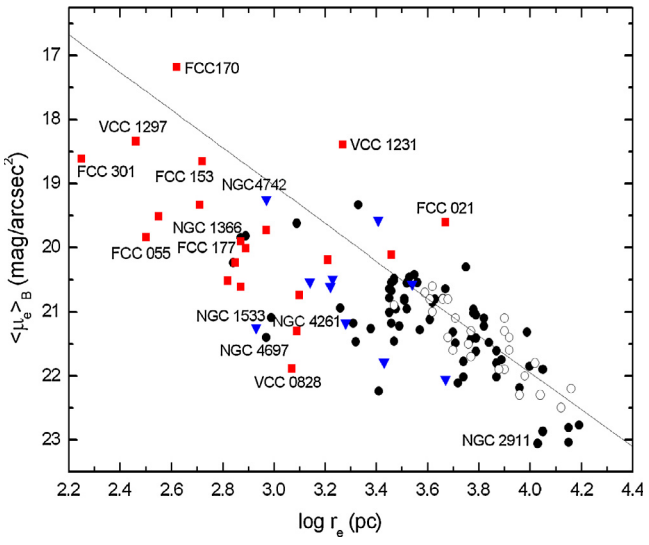

Figure 4 The Kormendy relation between the mean surface brightness $\langle\mu_e\rangle_B$ and effective radius r_e in the B band for ETGs. The solid line represents the Hamabe and Kormendy (1987) relation. The zero-point of the original relation has been shifted from V to the B-band assuming typical colors of B−V = 0.9. The symbols are as in Fig. 1.

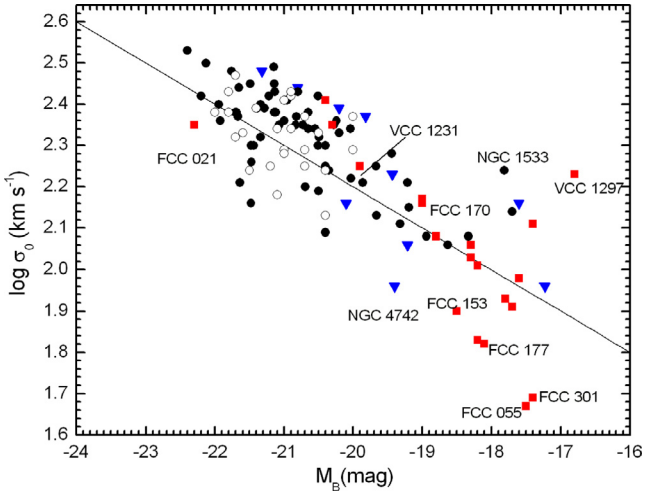

Figure 5 The $\log\sigma_o$ versus B-band absolute magnitude relation for our samples of ETGs. The straight line is the Faber–Jackson relation (FJR) for normal elliptical galaxies (Faber and Jackson, 1976). The symbols are as in Fig. 1.

that they have lower M/L ratios as expected for their young stellar populations. Also these galaxies have underestimated values of the central velocity dispersions which might affect on their positions relative to the FP.

The scatter of ETGs about the FP is correlated with age. Thus, we can introduce strong support for the idea that the position of an elliptical galaxy with respect to the FP is dependent on the time since its last starburst.

We found that the scatter about FJR is correlated with the post-merger age of the galaxy. Young ellipticals are brighter in the B band and/or have lower central velocity dispersion than the mean relation. The mean relation corresponds to galaxies that are ~10 Gyr old.

References

Annibali, F., Bressan, A., Rampazzo, R., Zeilinger, W.W., Vega, O., Panuzzo, P., 2010. Nearby early-type galaxies with ionized gas. IV. Origin and powering mechanism of the ionized gas. A&A 519, 40.

Auger, M.W., Treu, T., Bolton, A.S., Gavazzi, R., Koopmans, L.V. E., Marshall, P.J., Moustakas, L.A., Burles, S., 2010. The Sloan Lens ACS Survey. X. Stellar, dynamical, and total mass correlations of massive early-type galaxies. ApJ 724, 511.

Bamford, S.P. et al, 2009. Galaxy Zoo: the dependence of morphology and colour on environment. MNRAS 393, 1324.

Bender, R., 1988. Rotating and counter-rotating cores in elliptical galaxies. A&A 202, 5.

Bender, R., Burstein, D., Faber, S.M., 1992. Dynamically hot galaxies. I – structural properties. ApJ 399, 462.

Bennert, N., Canalizo, G., Jungwiert, B., Stockton, A., Schweizer, F., Peng, C.Y., Lacy, M., 2008. Evidence for merger remnants in early-type host galaxies of low-redshift QSOs. ApJ 677, 846.

Bernardi, M. et al, 2003. Early-type galaxies in the Sloan digital sky survey. II. Correlations between observables. AJ 125, 1849.

Binney, J., Tremaine, S., 2008. Galactic Dynamics, second ed. Princeton University Press.

Bolton, A.S., Treu, T., Koopmans, L.V.E., Gavazzi, R., Moustakas, L.A., Burles, S., Schlegel, D.J., Wayth, R., 2008. The Sloan Lens ACS Survey. VII. Elliptical galaxy scaling laws from direct observational mass measurements. ApJ 684, 248.

Borriello, A., Salucci, P., Danese, L., 2003. The fundamental plane of ellipticals – I. The dark matter connection. MNRAS 341, 1109.

Bosma, A., Smith, R.M., Wellington, K.J., 1985. Rotation and velocity dispersion in the stellar component of NGC 1316 (Fornax A). MNRAS 212, 301.

Bregman, J.D., Bregman, J.N., Temi, P., 2008. Unusual PAH emission in elliptical galaxies. ASPC 301, 34.

Bregman, J.D., Bregman, J.N., Temi, P., 2006a. The Spitzer Science Center 2005 Conference: Infrared Diagnostics of Galaxy Evolution, astro-ph/0604369.

Bregman, J.N., Temi, P., Bregman, J.D., 2006b. The ages of elliptical galaxies from infrared spectral energy distributions. ApJ 647, 265.

Burstein, D., Davies, R.L., Dressler, A., Faber, S.M., Stone, R.P.S., Lynden-Bell, D., Terlevich, R.J., Wegner, G., 1987. Spectroscopy and photometry of elliptical galaxies. III – UBV aperture photometry, CCD photometry, and magnitude-related parameters. ApJS 64, 601.

Calvi, R., Poggianti, B.M., Fasano, G., Vulcani, B., 2012. The distribution of galaxy morphological types and the morphology-mass relation in different environments at low redshift. MNRAS 419, L14.

Caon, N., Capaccioli, M., D'Onofrio, M., 1994. 'Global mapping' B-band photometry of a complete sample of Fornax and Virgo early-type galaxies. A&AS 106, 199.

Capaccioli, M., Longo, G., 1994. Kinematical properties of early-type galaxies. A&AR 5, 293.

Cappellari, M., et al., 2006. The mass-to-light ratio, the virial mass estimator and the Fundamental Plane of elliptical and lenticular galaxies, MNRAS, 366, 1126 The SAURON project – IV.

Cappellari, M. et al, 2013. The ATLAS3D project – XV. Benchmark for early-type galaxies scaling relations from 260 dynamical models: mass-to-light ratio, dark matter, Fundamental Plane and Mass Plane. MNRAS 432, 1709.

Carter, D., Jorden, P.R., Thorne, D.J., Wall, J.V., Straede, J.C., 1983. CCD surface photometry of two southern active galaxies, NGC 1316 and 1052. MNRAS 205, 377.

Collobert, M., Sarzi, M., Davies, R.L., Kuntschner, H., Colless, M., 2006. Central stellar populations of early-type galaxies in low-density environments. MNRAS 370, 1213.
Conselice, C.J., Mortlock, A., Bluck, A.F.L., Grützbauch, R., Duncan, K., 2013. Gas accretion as a dominant formation mode in massive galaxies from the GOODS NICMOS Survey. MNRAS 430, 1051.
de Carvalho, R.R., Djorgovski, S.G., 1992. Systematic differences between the field and cluster elliptical galaxies. ApJ 389, L49.
de la Rosa, I.G., de Carvalho, R.R., Zepf, S.E., 2001. The Fundamental Plane of elliptical galaxies in compact groups. AJ 122, 93, RC01.
Denicoló, G., Terlevich, R., Terlevich, E., Forbes, D.A., Terlevich, A., Carrasco, L., 2005a. Group, field and isolated early-type galaxies – I. Observations and nuclear data. MNRAS 356, 1440.
Denicoló, G., Terlevich, R., Terlevich, E., Forbes, D.A., Terlevich, A., 2005b. Group, field and isolated early-type galaxies – II. Global trends from nuclear data. MNRAS 358, 813, D05b.
de Vaucouleurs, G., de Vaucouleurs, A., Corwin, H.G., Buta, R.J., Paturel, G., Fouque, P., 1991. Book-review – third reference catalogue of bright galaxies. S&T 82, 621.
de Zeeuw, T., Franx, M., 1989. Kinematics of gas in a triaxial galaxy. ApJ 343, 617.
Djorgovski, S., Davis, M., 1987. Fundamental properties of elliptical galaxies. ApJ 313, 59.
D'Onofrio, M., Capaccioli, M., Zaggia, S.R., Caon, N., 1997. The relative distances to the Virgo, Fornax and Coma clusters of galaxies through the D_n-sigma and the Fundamental Plane relations. MNRAS 289, 847.
D'Onofrio, M., Zaggia, S.R., Longo, G., Caon, N., Capaccioli, M., 1995. Major axis kinematics of 15 early-type galaxies in the Fornax cluster. A&A 296, 319.
Dressler, A., 1980. Galaxy morphology in rich clusters – implications for the formation and evolution of galaxies. ApJ 236, 351.
Dressler, A., Lynden-Bell, D., Burstein, D., Davies, R.L., Faber, S. M., Terlevich, R., Wegner, G., 1987. Spectroscopy and photometry of elliptical galaxies. I – a new distance estimator. ApJ 313, 42.
Dressler, A., et al., 1997. Evolution since $z = 0.5$ of the Morphology-Density Relation for Clusters of Galaxies.
Faber, S.M., Dressler, A., Davies, R.L., Burstein, D., Lynden-Bell, D., 1987. In: Nearly Normal Galaxies. From the Planck Time to the Present; Proceedings of the Eighth Santa Cruz Summer Workshop in Astronomy and Astrophysics. Springer-Verlag, Santa Cruz, CA, New York, pp. 175–183.
Faber, S.M., Jackson, R.E., 1976. Velocity dispersions and mass-to-light ratios for elliptical galaxies. ApJ 204, 668.
Ferrarese, L., Ford, H.C., Jaffe, W., 1996. Evidence for a massive black hole in the active galaxy NGC 4261 from Hubble Space Telescope images and spectra. ApJ 470, 444.
Forbes, D.A., Ponman, T.J., 1999. On the relationship between age and dynamics in elliptical galaxies. MNRAS 309, 623.
Forbes, D.A., Ponman, T.J., Brown, R.J.N., 1998. Dependence of the Fundamental Plane scatter on galaxy age. ApJ 508, L43.
Fort, B.P., Prieur, J.-L., Carter, D., Meatheringham, S.J., Vigroux, L., 1986. Surface photometry of shell galaxies. ApJ 306, 110.
Franx, M., Illingworth, G., Heckman, T., 1989. Major and minor axis kinematics of 22 ellipticals. ApJ 344, 613.
Georgakakis, A., Hopkins, A.M., Caulton, A., Wiklind, T., Terlevich, A.I., Forbes, D.A., 2001. Cold gas in elliptical galaxies. MNRAS 326, 1431.
Gómez, P.L. et al, 2003. Galaxy star formation as a function of environment in the early data release of the Sloan digital sky survey. ApJ 584, 210.
Goudfrooij, P., de Jong, T., Hansen, L., Norgaard-Nielsen, H.U., 1994a. Interstellar matter in elliptical galaxies – part three – properties of dust extinction. MNRAS 271, 833.
Goudfrooij, P., Gilmore, D., Whitemore, B.C., Schweizer, F., 2004. Deep luminosity functions of old and intermediate-age globular clusters in NGC 1316: evidence for dynamical evolution of second-generation globular clusters. ApJ 613, L121.
Goudfrooij, P., Hansen, L., Jorgensen, H.E., Norgaard-Nielsen, H. U., 1994b. Interstellar matter in Shapley-Ames elliptical galaxies. II. The distribution of dust and ionized gas. A&AS 105, 341.
Graham, A., Colless, M., 1997. Some effects of galaxy structure and dynamics on the Fundamental Plane. MNRAS 287, 221.
Graham, A.W., Driver, S.P., 2005. A concise reference to (Projected) Sérsic R1/n quantities, including concentration, profile slopes, Petrosian Indices, and Kron Magnitudes. PASA 22, 118.
Gregg, M., 1992. Stellar population-induced peculiar velocities of elliptical galaxies. ApJ 384, 43.
Guzmán, R., Lucey, J.R., 1993. A new age-independent distance indicator for elliptical galaxies. MNRAS 263, L47.
Guzmán, R., Lucey, J.R., Bower, R.G., 1993. The fundamental relations of elliptical galaxies. MNRAS 265, 731.
Haines, C.P., Gargiulo, A., La Barbera, F., Mercurio, A., Merluzzi, P., Busarello, G., 2007. The different physical mechanisms that drive the star formation histories of giant and dwarf galaxies. MNRAS 381, 7.
Hamabe, M., Kormendy, J., 1987. Correlations between R/1/4 – law parameters for bulges and elliptical galaxies. In: de Zeeuw, T. (Ed.), Proc. IAU Symp., 127, Structure and Dynamics of Elliptical Galaxies. Reidel, Dordrecht, p. 379.
Holden, B.P., van der Wel, A., Kelson, D.D., Franx, M., Illingworth, G.D., 2010. M/L_B and color evolution for a deep sample of Msstarf cluster galaxies at $z \sim 1$: the formation epoch and the tilt of the Fundamental Plane. ApJ 724, 714.
Ibarra-Medel, H.J., López-Cruz, O., 2011. XIII Latin American Regional IAU, Meeting. In: Henney, W.J., Torres-Peimbert, S. (Eds.), Revista Mexicana de Astronomía y Astrofísica (Serie de Conferencias), The Universality of the Fundamental Plane for Galaxies and Galaxy Systems: M/L, vol. 40, pp. 64.
Jaffe, W., Ford, H.C., Ferrarese, L., van den Bosch, F., O'Connell, R. W., 1993. A large nuclear accretion disk in the active galaxy NGC4261. Nature 364, 213.
Jaffe, W., Ford, H., Ferrarese, L., van den Bosch, F., O'Connell, R. W., 1996. The nuclear disk of NGC 4261: Hubble Space Telescope images and ground-based spectra. ApJ 460, 214.
Janowiecki, S., Mihos, J.C., Harding, P., Feldmeier, J.J., Rudick, C., Morrison, H., 2010. Diffuse Tidal Structures in the Halos of Virgo Ellipticals. ApJ 715, 972.
Jørgensen, I., Franx, M., Kjærgaard, P., 1996. The FUNDAMENTAL PLANE for cluster E and S0 galaxies. MNRAS 280, 167.
Jørgensen, I., Franx, M., Kjærgaard, P., 1993. Sources of scatter in the Fundamental Plane and the Dn-sigma relation. ApJ 411, 34.
Koleva, M., Prugniel, P., de Rijcke, S., Zeilinger, W.W., 2011. Age and metallicity gradients in early-type galaxies: a dwarf-to-giant sequence. MNRAS 417, 1643.
Kuntschner, H., 2000. The stellar populations of early-type galaxies in the Fornax cluster. MNRAS 315, 184.
Kuntschner, H., Smith, R.J., Colless, M., Davies, R.L., Kaldare, R., Vazdekis, A., 2002. The stellar populations of early-type galaxies in the Fornax cluster. MNRAS 337, 172.
La Barbera, F., de Carvalho, R.R., de la Rosa, I.G., Lopes, P.A.A., 2010a. SPIDER – II. The Fundamental Plane of early-type galaxies in grizYJHK. MNRAS 408, 1335.
La Barbera, F., Lopes, P.A.A., de Carvalho, R.R., de la Rosa, I.G., Berlind, A.A., 2010b. SPIDER – III. Environmental dependence of the Fundamental Plane of early-type galaxies. MNRAS 408, 1361.
Lauberts, A., Valentijn, E.A., 1989. The data of the surface photometry catalogue of the ESO-Uppsala galaxies are now available. Msngr 56, 31.
Lewis, I. et al, 2002. The 2dF Galaxy Redshift Survey: the environmental dependence of galaxy star formation rates near clusters. MNRAS 334, 673.
Lucey, J.R., Bower, R.G., Ellis, R.S., 1991. The fundamental plane of cluster elliptical. MNRAS 249, 755.

Magoulas, C. et al, 2012. The 6dF Galaxy Survey: the near-infrared Fundamental Plane of early-type galaxies. MNRAS 427, 245.
Mahabal, A., Kembhavi, A., Singh, K.P., Bhat, P.N., Prabhu, T.P., 1996. A dust lane in the radio galaxy 3C 270. ApJ 457, 598.
Malin, D.F., Carter, D., 1980. Giant shells around normal elliptical galaxies. Nature 285, 643.
Mármol-Queraltó, E. et al, 2009. Evidence for intermediate-age stellar populations in early-type galaxies from K-band spectroscopy. ApJ 705, 199.
Michard, R., Prugniel, P., 2004. Peculiarities and populations in elliptical galaxies. I. An old question revisited. A&A 423, 833.
Nipoti, C., Londrillo, P., Ciotti, L., 2003. Galaxy merging, the fundamental plane of elliptical galaxies and the MBH-σ0 relation. MNRAS 342, 501.
Nowak, N., Saglia, R.P., Thomas, J., Bender, R., Davies, R.I., Gebhardt, K., 2008. The supermassive black hole of FornaxA. MNRAS 391, 1629.
Pahre, M.A., De Carvalho, R.R., Djorgovski, S.G., 1998. Near-infrared imaging of early-type galaxies. IV. The physical origins of the fundamental plane scaling relations. AJ 116, 1606.
Pinkney, J., Gebhardt, K., Richstone, D., Team, Nuker., 2000. Kinematics of early-type galaxies from the Nuker sample. AAS 196, 2109.
Pinkney, J. et al, 2003. Kinematics of 10 early-type galaxies from Hubble Space Telescope and ground-based spectroscopy. ApJ 596, 903.
Postman, M., Geller, M.J., 1984. The morphology-density relation – the group connection. ApJ 281, 95.
Postman, M. et al, 2005. The morphology-density relation in $z \sim 1$ clusters. ApJ 623, 721.
Rampazzo, R., Panuzzo, P., Vega, O., Marino, A., Bressan, A., Clemens, M.S., 2013. A Spitzer-IRS spectroscopic atlas of early-type galaxies in the Revised Shapley-Ames Catalog. MNRAS 432, 374.
Reda, F.M., 2007. Ph. D. thesis. Faculty of Information and Communication Technology, Swinburne University of Technology.
Reda, F.M., Forbes, D.A., Hau, G.K.T., 2005. The fundamental plane of isolated early-type galaxies. MNRAS 360, 693.
Renzini, A., 2006. Stellar population diagnostics of elliptical galaxy formation. ARA&A 44, 141.
Renzini, A., Ciotti, L., 1993. Transverse dissections of the fundamental planes of elliptical galaxies and clusters of galaxies. ApJ 416, L49.
Sambhus, N., Gerhard, O., Mendez, R.H., 2006. Kinematic evidence for different planetary nebula populations in the elliptical galaxy NGC 4697. AJ 131, 837.
Sánchez-Blázquez, P., Gorgas, J., Cardiel, N., Cenarro, J., González, J.J., 2003. Differences in carbon and nitrogen abundances between field and cluster early-type galaxies. ApJ 590, L91.
Sánchez-Blázquez, P., Gorgas, J., Cardiel, N., Gonzalez, J.J., 2006. Stellar populations of early-type galaxies in different environments. I. Line-strength indices. Relations of line-strengths with σ. A&A 457, 787.
Sandage, A., Tammann, G.A., 1987, A revised Shapley-Ames Catalog of bright galaxies, 2nd ed., Carnegie Institution of Washington Publication, Washington: Carnegie Institution, 1987.
Schweizer, F., 1980. An optical study of the giant radio galaxy NGC 1316/Fornax A/. ApJ 237, 303.
Schweizer, F., 1981. Optical properties of central region of NGC 1316 – a small bright core in a giant D galaxy. ApJ 246, 722.
Schweizer, F., Seitzer, P., 1992. Correlations between UBV colors and fine structure in E and S0 galaxies – a first attempt at dating ancient merger events. AJ 104, 1039.
Schweizer, F., Seitzer, P., Faber, S.M., Burstein, D., Dalle Ore, C.M., Gonzalez, J.J., 1990. Correlations between line strengths and fine structure in elliptical galaxies. ApJ 364, L33.
Silva, D.R., Kuntschner, H., Lyubenova, M., 2008. A new approach to the study of stellar populations in early-type galaxies: K-band spectral indices and an application to the Fornax Cluster. ApJ 674, 194.
Spolaor, M., Kobayashi, C., Forbes, D.A., Couch, W.J., Hau, G.K.T., 2010. Early-type galaxies at large galactocentric radii – II. Metallicity gradients and the [Z/H]-mass, [α/Fe]-mass relations. MNRAS 408, 272.
Tal, T., van Dokkum, P.G., Nelan, J., Bezanson, R., 2009. The frequency of tidal features associated with nearby luminous elliptical galaxies from a statistically complete sample. AJ 138, 1417.
Terlevich, A.I., Forbes, D.A., 2002. A catalogue and analysis of local galaxy ages and metallicities. MNRAS 330, 547, TF02.
Thomas, D., Maraston, C., Bender, R., Mendes de Oliveira, C., 2005. The epochs of early-type galaxy formation as a function of environment. ApJ 621, 673.
Tully, R.B., 1988. Nearby Galaxies Catalog. Cambridge Univ. Press, Cambridge.
Whitmore, B.C., McElroy, D.B., Schweizer, F., 1987. The shape of the dark halo in polar-ring galaxies. ApJ 314, 439.
Yuan, F., Yu, Z., Ho, L.C., 2009. Revisiting the "Fundamental Plane" of black hole activity at extremely low luminosities. ApJ 703, 1034.